

Optimization of a Bonse–Hart instrument by suppressing surface parasitic scattering

Michael Sztucki, Jacques Gorini, Jean-Pierre Vassalli, Loys Goirand,
Pierre van Vaerenbergh and Theyencheri Narayanan*

European Synchrotron Radiation Facility, BP 220, 38043 Grenoble, France. E-mail: narayan@esrf.fr

An improved crystal design for a Bonse–Hart ultra-small-angle scattering instrument is presented. Defects at the diffracting surfaces of the conditioning crystals were found to be at the origin of diffuse scattering that enhances the intensity in the wings of the rocking curves by several orders of magnitude. In order to improve the performance of the instrument, the monolithic channel-cut crystals were replaced by pairs of separate polished and deeply etched crystals. These crystals were mounted on a mechanical stage that allows very precise parallel alignment of the crystals to within a tiny fraction of the rocking curve width (sub- μ rad range). By using these double-crystal set-ups, the parasitic background scattering was reduced by more than an order of magnitude. The steps to achieve the optimum surface quality of the crystals as well as the precision mechanical design for their parallel alignment are described. Significant improvement of the signal-to-background ratio and the available wavevector range of the instrument make it suitable for studying the microstructure and dynamics of dilute and weakly scattering soft-matter systems. This development also has potential applications in X-ray optics such as low-background and tunable monochromators and collimators.

© 2008 International Union of Crystallography

Printed in Singapore – all rights reserved

Keywords: USAXS; Bonse–Hart optics; mechanically fabricated channel-cut crystals.

1. Introduction

The Bonse–Hart camera (Bonse & Hart, 1965, 1966) is an established set-up for ultra-small-angle X-ray scattering (USAXS) experiments (Long *et al.*, 1991; Pedersen, 1995). At synchrotron undulator sources the loss of intensity due to the finite acceptance of the channel-cut crystals is less important as the typical beam divergence is comparable with the width of the reflectivity curves of Si 111 crystals. On the other hand, the instrument offers the possibility of recording small-angle X-ray scattering (SAXS) over a wide dynamic range both in scattering vector \mathbf{q} and in intensity $I(q)$ (Diat *et al.*, 1995; Konishi & Ise, 1998; Ilavsky *et al.*, 2002; Pontoni & Narayanan, 2003). With the recent improvements, the low q limit has been extended to 0.001 nm^{-1} (with 12.4 keV X-rays), while offering a dynamic range over effectively more than eight orders of magnitude in intensity depending on the scattering power of the sample. The set-up also offers a high angular resolution (corresponding to a q resolution $\leq 0.001 \text{ nm}^{-1}$) which is limited mainly by the width of the rocking curves. Compared to a conventional pinhole camera, the Bonse–Hart set-up is not limited by the characteristics of currently available two-dimensional detectors (*e.g.* angular resolution and intensity dynamic range) (Pontoni *et al.*, 2002). Measurements are self-calibrated as the scattered intensity is directly determined in absolute units.

Certainly, Bonse–Hart USAXS is a complementary technique to high-resolution pinhole SAXS, which has certain advantages (Yagi & Inoue, 2003; Petukhov *et al.*, 2006). With the latter, the whole scattering pattern is recorded simultaneously and in a short time. This is an advantage for the investigation of oriented and radiation-sensitive specimens as well as time-resolved experiments. Nevertheless, Bonse–Hart USAXS has found some unique applications in colloid science (Harada *et al.*, 2000; Lyonnard *et al.*, 2000; Pontoni *et al.*, 2003; Beaucauge, Kammler & Pratsinis, 2004; Narayanan *et al.*, 2006).

The maximization of the signal-to-background ratio is an important goal for enhancing the performance of Bonse–Hart USAXS. Thereby, it becomes feasible to investigate weakly scattering and low-contrast samples and to increase the available q range of the instrument (Sztucki *et al.*, 2007). In this respect, the main limitation arises from the parasitic scattering contributions to the wings of the rocking curves of the channel-cut crystals employed in the Bonse–Hart set-up. The observed scattering deviates considerably from the calculations based on the dynamical theory of diffraction. This has been explained by the limited surface quality of monolithic channel-cut crystals (Agamalian *et al.*, 1998).

In this article, recent developments in the Bonse–Hart set-up installed at the high-brilliance beamline ID2 (Narayanan *et al.*, 2001) at the European Synchrotron Radiation Facility (ESRF) in Grenoble, France, are presented. The improvement

in the crystal design that allowed a reduction of the parasitic scattering background by more than an order of magnitude is discussed in detail. Scientific examples demonstrate the feasibility of ultra-small-angle X-ray scattering experiments with dilute and low-contrast samples. In addition, the suitability of the improved technology for the design of future X-ray optics is discussed.

2. Experimental set-up

2.1. Beamline description

Fig. 1 shows the schematic layout of the USAXS Bense–Hart camera at ID2. The undulators located at a high- β section of the storage ring provide high photon flux with low beam divergence. The beamline optics consist of a cryogenically cooled Si-111 channel-cut monochromator and a Rh-coated double-focusing toroidal mirror deflecting the X-ray beam vertically. The standard beam size defined by the secondary slits is $300\ \mu\text{m} \times 300\ \mu\text{m}$ full width at half-maximum (FWHM).

The ID2 USAXS set-up makes use of triple-bounce Si-220 channel-cut crystals as an analyzer and conditioning crystal that deflects the beam horizontally. This allows easy switching between the Bense–Hart configuration and the SAXS/WAXS pinhole camera within the span of a few minutes by turning the Si-220 conditioning crystal. Therefore, both instruments can be used in a complementary manner.

The first Si-220 crystal set-up is crossed (orthogonal) with the Si-111 channel-cut monochromator of the beamline optics and serves primarily for horizontal beam conditioning. The scattered intensity is analyzed by a set of two channel-cut crystals, a triple-bounce Si-220 horizontal crystal and an orthogonal double-reflection Si-111 vertical analyzer which is usually maintained at the corresponding Bragg angle. The crossed configuration of the analyzer crystals eliminates the well known problem of de-smearing of the Bense–Hart set-up, providing directly the high-resolution scattering profiles in point collimation.

The first analyzer crystal can be rocked in linear or logarithmic steps with a step size of $\sim 0.2\ \mu\text{rad}$ to obtain the scattering profile as a function of the modulus of the scattering vector, $|\mathbf{q}| = (4\pi/\lambda)\sin(\theta/2)$, where λ is the incident wavelength and θ is the scattering angle. During a scan of the horizontal analyzer, the crossed analyzer and detector are positioned to be centered with respect to the exiting beam.

The beam path up to the sample position is kept under vacuum, whereas the analyzer crystals are operated in air. The thin mica window which separates the vacuum in the incident section and sample stage is used as a scattering reference for an incident beam monitor. High-dynamic-range

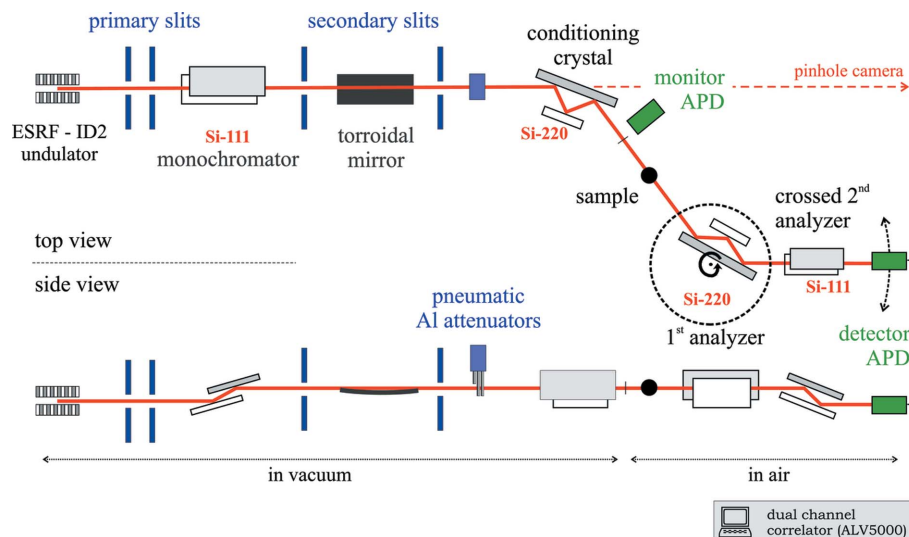


Figure 1 Schematic layout of the USAXS Bense–Hart camera installed at beamline ID2, ESRF. The first Si-220 crystal is primarily used for horizontal beam conditioning. The scattered intensity is measured by scanning the first horizontal analyzer crystal together with the second vertical analyzer (maintained at the Bragg angle) and detector which are centered with respect to the exiting beam.

($\sim 3 \times 10^7$ counts s^{-1}) avalanche photodiodes (APDs) operated in photon counting mode are used for both monitor and detector. A further increase of the total dynamic range of intensity is achieved by the use of fast pneumatically controlled Al attenuators installed before the Si-220 conditioning crystal which automatically optimize the count rates on the detector during a scan. They are also used to protect the sample from radiation damage. With this set-up, scans over typically 11 orders of magnitude in intensity can be recorded.

The Bense–Hart camera is presently optimized for a fixed wavelength around 0.1 nm (12.4 keV). However, provision is made to operate up to 16 keV (~ 0.077 nm). Owing to the improved design of the conditioner and analyzer described in the next paragraph, the set-up provides a useful q range of $0.001\ \text{nm}^{-1} < q < 1\ \text{nm}^{-1}$ at 12.4 keV. High-quality rocking curves up to 5 mrad ($\sim 0.3\ \text{nm}^{-1}$) can be usually recorded within an acquisition time of less than 4 min. The scans are reproducible within about $1\ \mu\text{rad}$. Because of the high flux [photon flux at the sample position is of the order of 10^{12} photons s^{-1} (100 mA ring current) $^{-1}$], low beam divergence and high dynamic range detection, fast scans can be performed in less than a minute, permitting limited time-resolved USAXS measurements. Taking into account that dynamics is slower at small wavevectors, this time-resolution is adequate in many cases to study kinetics at relatively large length scales (Pontoni & Narayanan, 2003).

For typical static experiments, the central part of the rocking curve is measured in an initial linear scan ($\pm 20\ \mu\text{rad}$) which then continues in logarithmic steps to acquire the desired range of the scattering curve. As a result, the direct beam position, the width of the rocking curve and the transmitted intensity, I_T , are registered and verified for each scan. The scattered intensity, $I_S(q)$, is directly converted to an absolute scale without any scaling factor or secondary stan-

dards using the widths of rocking curves of the horizontal and the vertical analyzer crystals measured without the sample.

Fig. 2(a) illustrates the principle of the Bonse & Hart (1965, 1966) based USAXS set-up and the procedure for absolute intensity calibration by means of a schematic scattering pattern. Both analyzer crystals cut out orthogonal slices from the two-dimensional scattering profile. Their cross section (point collimation) defines the solid angle, $\Delta\Omega$, which is scanned along the horizontal q_x direction by rotating the first analyzer crystal.

Fig. 2(b) shows the typical horizontal rocking curve normalized to the transmitted intensity I_T . The horizontal rocking curve of the set-up is defined by the convolution of the reflectivity curves R_1 and R_2 of the beam conditioning and analyzer crystals (Darwin curves) according to

$$I(\Delta) = \int R_1^n(y)R_2^m(y + \Delta) dy, \quad (1)$$

where n and m are the numbers of reflections in the horizontal first conditioning monochromator and the first analyzer crystal, respectively. The use of multiple reflection results in a suppression of the far-reaching wings of the rocking curve. For the depicted triple-bounce set-up, a decay $q^{-2 \times 3} \rightarrow q^{-6}$ is expected. In reality, the shape of the rocking curves deviates from the predictions of dynamical theory owing to parasitic contributions (see next paragraph). The measured FWHM is about 14.5 μrad . The second analyzer crystal is usually kept at the maximum of the Bragg condition. The alignment scan along this vertical scattering direction is shown in Fig. 2(c). In this direction, no cleaning of the beam is carried out and the width of the rocking curve is mainly determined by the beam divergence convoluted by the width of the Si-111 rocking curve, resulting in a FWHM of about 45 μrad . The absolute scattered intensity [the differential scattering cross section per unit volume, $d\Sigma/d\Omega$ or $I(q)$] is derived from

$$\frac{d\Sigma}{d\Omega} = I(q) = \frac{I_S(q)}{I_0 A E T_r t \Delta\Omega}, \quad (2)$$

where I_0 is the incident flux, A is the beam cross section, E is the detector efficiency, T_r is the sample transmission, t is the known sample thickness, and $\Delta\Omega$ is the solid angle defined by the width of the rocking curves of the two analyzer crystals. $I_0 A E T_r = I_T$ is automatically measured for each scan.

The scattering intensity of the sample is superimposed on the rocking curve recorded without sample. Fig. 3(a) shows such an ‘empty’ rocking curve together with the measurement

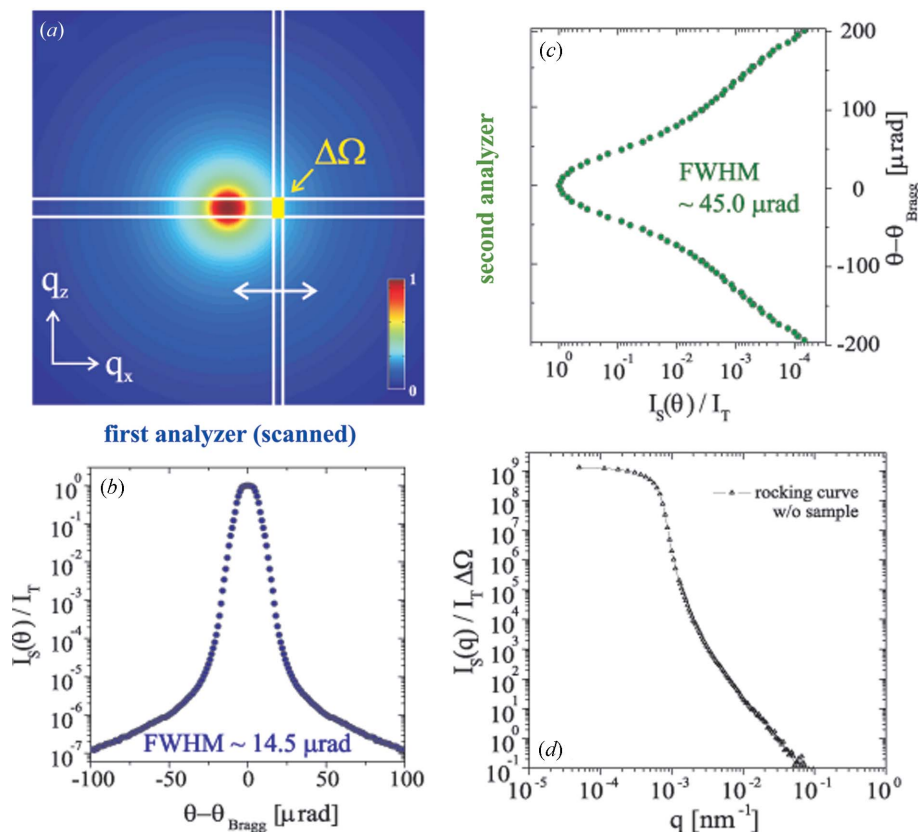


Figure 2

(a) Schematic scattering pattern: first and second analyzer crystals cut out orthogonal slices from the two-dimensional scattering profile defining the solid angle, $\Delta\Omega$ (point collimation). (b) Typical rocking curve recorded with the first (horizontal) analyzer set-up normalized to the transmitted intensity I_T . (c) Rocking curve of the second (vertical) analyzer crystal. (d) Typical rocking curve recorded without sample on a double-logarithmic scale.

of scattering for a suspension of spherical silica particles (radius ~ 300 nm) in water.

The background of the empty rocking curve is subtracted from the measurement of the sample. $I(q)$ in absolute units is obtained after normalization of transmission and subsequent division by $\Delta\Omega$ and sample thickness (see Fig. 3b). The high-resolution scattering profile spans over a dynamic range of effectively more than seven orders of magnitude in intensity. To demonstrate the high angular resolution of the Bonse–Hart set-up (corresponding to a q resolution of ~ 0.001 nm^{-1}), pinhole SAXS data recorded at a sample-to-detector distance of 10 m are shown for comparison. The two-dimensional SAXS patterns were recorded with a high-sensitivity fiber-optically coupled CCD detector (FReLoN) with an effective dynamic range of 32000. To obtain the full dynamic range, the pinhole SAXS data are combined from two sets with and without using a circular absorber close to the beamstop. After azimuthal integration, the two data sets were combined to cover the indicated dynamic range in intensity. The large number of oscillations at higher q values depict the form factor of almost monodisperse spherical particles while the peak near $q \simeq 0.01$ nm^{-1} arises from the structure factor of interparticle interactions (Sztucki *et al.*, 2006). Fig. 3(b) highlights the importance of Bonse–Hart measurements even in the q range which is accessible to pinhole SAXS. The higher

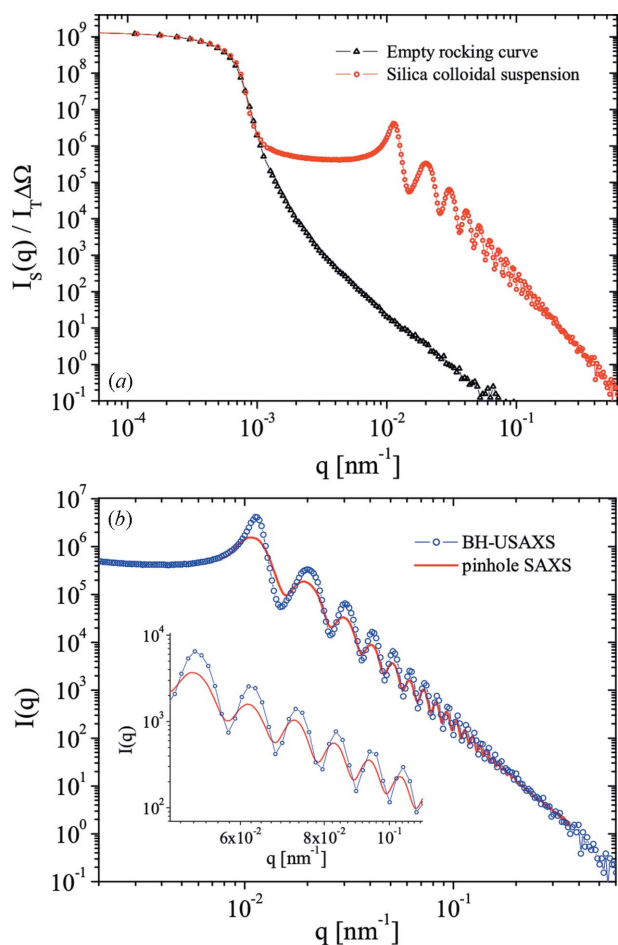


Figure 3
 (a) Typical intensity of a rocking curve recorded without sample together with the scattering of a suspension of spherical silica particles (radius ~ 300 nm) in water. (b) High-resolution $I(q)$ data in absolute units after background subtraction: the Bonse–Hart intensity range spans over more than seven orders of magnitude. For a comparison, data recorded with a pinhole SAXS instrument are also shown. The inset shows a zoom into the observed form factor of spherical particles.

resolution of the Bonse–Hart set-up is especially important for unambiguously separating the form and structure factors.

Optionally, the coherent part of the beam can be selected with a small slit setting (typically $0.02\text{ mm} \times 0.02\text{ mm}$) allowing dynamic X-ray scattering measurements to be performed (Sztucki & Narayanan, 2007). In this configuration the parasitic scattering from the slits is effectively curtailed by the first conditioning crystal. This provides access to very low q values using 12.4 keV X-rays. A significant improvement in the signal-to-background ratio is also important for deriving a proper homodyne intensity autocorrelation function, $g_T^{(2)}(q, t)$, without possible heterodyning effects. Moreover, it should be emphasized that both static and dynamic USAXS measurements can be recorded within a single experimental set-up.

The Bonse–Hart USAXS instrument also offers sufficient flexibility concerning the installation of sample environments providing about 0.5 m space between the monitor APD and the vacuum vessel of the first analyzer crystal. Control of the instrument is realised using few commands under *SPEC* software (Certified Scientific Software). For on-line data

reduction and analysis, a graphical user interface has been developed under *Matlab* (Sztucki & Narayanan, 2007). The software allows direct import from *SPEC* output files. The data are automatically background subtracted, converted to calibrated curves in absolute units, and can be exported in ASCII format. Tools for averaging, binning and subtraction are supplied. The program has standard plotting and printing features implemented and can be used for visualization of any small-angle scattering data, in particular allowing for a direct online comparison of pinhole SAXS and Bonse–Hart USAXS measurements. Furthermore, a fitting routine for polydisperse form and structure factor models has also been implemented (Sztucki, 2007).

2.2. Optimization of crystal design

The principle of the USAXS set-up proposed by Bonse & Hart (1965, 1966) is the suppression of the far-reaching wings of the rocking curves by means of multiple reflections using channel-cut crystals. However, parasitic scattering observed in this part of the rocking curves exceeds the predictions of the dynamical theory of diffraction by several orders of magnitude (see Fig. 5).

Previous studies (Agamalian *et al.*, 1998) have shown that ultra-small-angle scattering from the surface microstructure of the crystals is at the origin of the observed departure from dynamical diffraction theory. Owing to the limited surface quality, a network of cracks remains in the surface layer of the monolithic channel-cut crystals resulting in parasitic contributions to the wings of the rocking curves.

Therefore, the idea was to replace the monolithic channel-cut crystals by pairs of independent parallel crystals. In this case, mechanical polishing and etching of the crystal surface is facilitated allowing a better surface finish. The crystals in this configuration, henceforth referred to as the double-crystal set-up, are mounted on a mechanical stage that allows very precise alignment. Thereby, it is possible to improve the signal-to-background ratio of the existing Bonse–Hart set-up which in turn permits investigation of dilute and low-contrast samples as well as to increase effectively the available q range of the instrument.

2.2.1. Mechanical set-up for precise crystal alignment. The first step was the design of a mechanical support of the crystals. The precision (sub- μrad resolution) and high stability of this set-up should allow aligning and maintaining a pair of crystals to the same degree as in a monolithic channel-cut crystal.

Fig. 4 shows the design of the triple-bounce double-crystal arrangement. The installed crystal pair is shown semi-transparent to allow the visualization of the X-ray beam trajectory including the three reflections. To achieve larger exit angles without shadowing of the scattered intensity by the edge of the crystal during a scan, the length of the crystal in front is reduced.

The support together with the long crystal is fixed on a motorized rotation stage (not shown) to turn to the desired scattering angle with $\sim 0.2\ \mu\text{rad}$ resolution. The small crystal

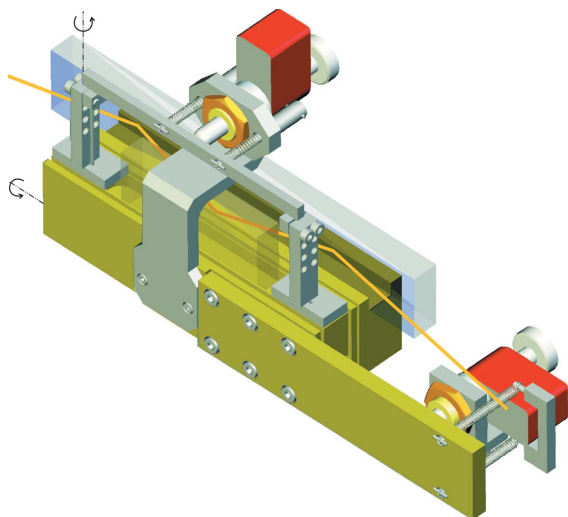


Figure 4

Design of the double-crystal set-up. The precise and stable alignment of the Bragg condition (sub- μ rad accuracy) is assured by the piezoelectric actuator (picomotor, Newfocus) on the long lever (right). An additional horizontal tilt stage (picomotor on top) is used for initial alignment of the set-up (beam height). The pair of polished and deeply etched crystals is shown semi-transparent to visualize the X-ray beam trajectory including three reflections.

in front can be aligned relative to the long crystal around the vertical and horizontal axes in order to achieve the performance of a monolithic channel-cut crystal. The precise and stable alignment of the Bragg condition around the vertical axis with sub- μ rad accuracy is assured by the piezoelectric actuator (picomotor, Newfocus) on the long lever in front. To reduce the space requirements, the center of this tilt stage is situated at the (left) border of the system. The resulting change of the channel width is negligible taking into account the tiny changes of angle. An additional horizontal tilt stage using the picomotor on top of the system is used for alignment of the horizontal trajectory of the beam through the channel. This tilt stage is less sensitive and mainly used for initial alignment of the set-up.

The mechanical stability and reproducibility of the described system is extremely good. However, regular realignment of the Bragg condition (tilt around vertical axis) using the picomotor on the long lever is performed. An eventual misalignment of the crystals is easily detected in a reduction of the maximum transmitted intensity and change of the shape of the rocking curves measured without sample (faster decay from the central plateau of the rocking curve).

2.2.2. Preparation of crystal surface. The most important advancement was the preparation of Si-220 crystals with the best possible surface finish in the crystal laboratory at the ESRF. After machining of the crystals from the Si ingot, the crystals were etched for 5 min in a mixture of nitric acid (65%) and hydrofluoric acid (48%) with a ratio of 4:1 by volume. This was followed by an optical polishing using diamond powder of size 1 μ m, suspended in alcohol. This reduces the surface roughness to about 40 \AA . A further reduction to typically ~ 5 \AA is achieved by mechano-chemical polishing using a colloidal suspension of silica (Ludox, PW30, silica particles

with 30 nm mean particle size). The best results for the double-crystal set-up are achieved after a further important etching for 15 min with a mixture of nitric acid and hydrofluoric acid in a ratio of 15:1. After this treatment, the optical surface of the crystals shows a light orange-peel surface texture which might reduce the quality of the crystals for use in imaging applications. On the other hand, for the scattering application, it shows very good performance especially regarding the significant reduction of the diffuse scattering background in the wings of the rocking curves and the conservation of beam coherence. The improvements obtained after the etching procedure are attributed to the removal of slightly misaligned crystallites on the crystal surface owing to the mechanical polishing (Agamalian *et al.*, 1998).

Fig. 5 presents the improvement in the parasitic scattering background in the wings of the (horizontal) rocking curve obtained using two sets of polished and deeply etched flat crystals which are precisely aligned parallel to each other. For a comparison, the rocking curve obtained with the original monolithic channel-cut crystals is also shown. The continuous line indicates the rocking curve calculated by the dynamical theory of diffraction. For this purpose, the Darwin reflectivity curve R of a Si-220 crystal was calculated using the program *XOP* (Sánchez del Río & Dejus, 1997). According to equation (1), a decay $q^{-2 \times 3} \rightarrow q^{-6}$ is expected for the depicted triple-bounce set-up (see logarithmic representation in the inset of Fig. 5).

As shown in Fig. 5, the parasitic scattering background in the wings of the rocking curve could be suppressed by more than an order of magnitude by the improved design. The result is much closer to the theoretical prediction as compared with the standard set-up and subsequent etching of the crystals did not improve the background level. However, to understand

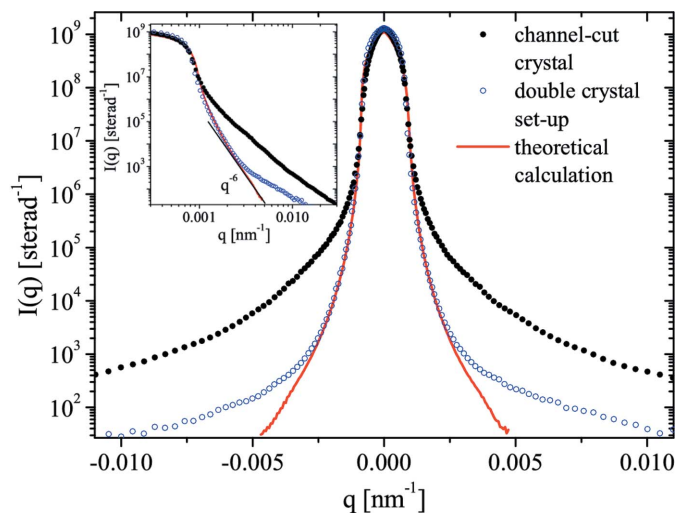


Figure 5

Comparison of rocking curves obtained using monolithic channel-cut crystals and double-crystal devices consisting of two parallel polished and deeply etched crystals. The parasitic scattering background in the wings of the rocking curve could be reduced by more than an order of magnitude using the latter. The continuous line indicates the rocking curve calculated by the dynamical theory of diffraction. The logarithmic representation in the inset emphasizes the expected q^{-6} decay which is followed by the experimental curve up to $q \simeq 0.0023 \text{ nm}^{-1}$.

the origin of the remaining background we investigated by putting the whole system, including sample position and the first analyzer stage, under vacuum avoiding any windows in front of the analyzer crystals. The measured rocking curves did not improve significantly which suggests that the residual parasitic scattering could be originating from the remaining surface defects, and possibly the thermal diffuse scattering from the bulk.

In order to improve the stability of the camera, replacing the new double-crystal set-up in the first analyzer stage with a deeply etched monolithic channel-cut crystal ('hybrid system') was tested. These investigations, involving four iterations of successive etching, demonstrate very well the importance of the polishing and etching procedure of the two pairs of crystals (see Figs. 6 and 7). The tests were performed using an optimized double-crystal system as horizontal conditioning crystal

and were therefore not affected by the change of two crystal sets at the same time.

The fabrication of the monolithic Si-220 channel-cut crystal corresponds essentially to the production of the flat crystals, described above. Solely, the mechano-chemical etching cannot be performed owing to the geometrical constraints of the narrow channel.

Fig. 6 shows the evolution of the parasitic scattering background as a function of etching time of the first analyzer crystal on a double-logarithmic scale. The parasitic scattering background after an etching with nitric acid and hydrofluoric acid in a ratio of 10:1 for 10 min after optical polishing is comparable with the scattering derived from the pair of monolithic channel-cut crystals originally used in the set-up (not shown). A significant improvement is achieved by a further etching step for 10 min at a concentration of 15:1. Repeating the same treatment another time resulted in a reduction of the parasitic background, especially in the range of the smaller q values. Beyond that limit, subsequent etching neither improved the background level further nor deteriorated it noticeably.

Fig. 7 compares the rocking curve derived using the optimized hybrid system discussed above with the best rocking curve measured with a system using two double-crystal set-ups for both conditioning and analyzer crystals. The obtained results are amazingly similar. Therefore, the currently used Bense–Hart set-up uses the new double-crystal set-up only as conditioning crystal. The maintenance-free deeply etched monolithic channel-cut crystal is employed as first analyzer.

The importance of the mechano-chemical polishing of the horizontal conditioning crystal becomes evident when the crystal set-ups used for beam conditioning and first analyzer were interchanged; that is, when the deeply etched monolithic channel-cut crystal is installed as conditioning crystal and the optimized double-crystal set-up works as first analyzer ('reverse combination'). In this case the resulting rocking curve (see Fig. 7, dotted line) manifests an extremely high parasitic scattering background. From this, it can be concluded that for a low-background Bense–Hart set-up it is indispensable to use highly polished and deeply etched conditioning crystals. This is due to the fact that the conditioning crystal is always in the Bragg condition and the parasitic background originating from the last bounce superimposes directly on the sample scattering. In addition, the apparent width of the rocking curve of the conditioning crystal is convoluted by the horizontal beam divergence and therefore has a much larger bandpass for the parasitic background. For the analyzer stage the crystalline quality is more important than the microscopic surface roughness. Therefore, deep etching of the analyzer crystals is sufficient to reach optimal conditions.

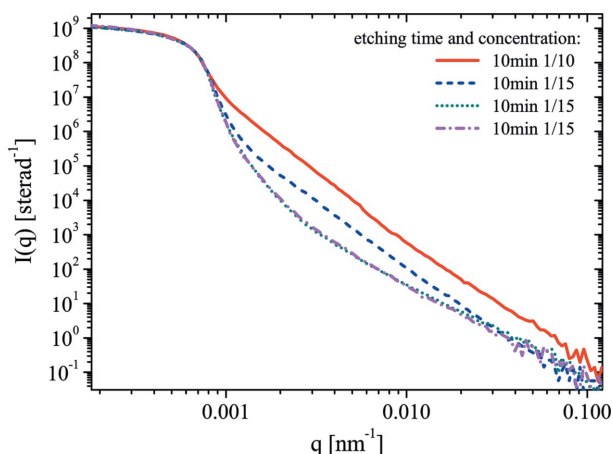


Figure 6 Evolution of the parasitic scattering background as a function of etching time of the first analyzer crystal after optical polishing. Here a monolithic Si-220 channel-cut crystal is used, whereas a Si-220 double-crystal set-up is installed as conditioning crystal ('hybrid system'). After the third etching, the background level did not improve any further. The concentrations are given as the volume ratio of hydrofluoric acid and nitric acid.

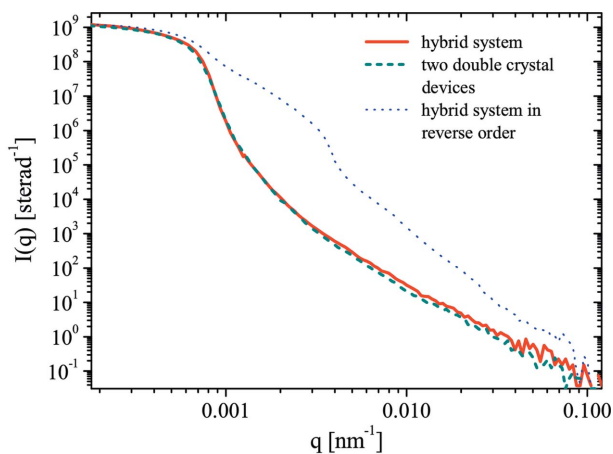


Figure 7 Comparison of rocking curves derived from the hybrid system, double-crystal devices for both conditioner and analyzer, and the hybrid system installed in the reverse order (see text for more details).

3. Scientific applications

The improved Bense–Hart set-up has a lower scattering background than an optimized pinhole SAXS camera (q range 0.001–0.2 nm⁻¹) and thereby provides new opportunities for

probing the structure and dynamics of soft matter in the ultra-small-angle range.

3.1. *In situ* study of growth dynamics of soot particles

Soot formation is an important topic in environmental science. In addition, controlled aggregations of nanometric particles are involved in many industrial processes. The investigation of the growth dynamics of soot particles in hydrocarbon-fuelled flames is a challenging issue owing to the rapid nucleation and growth conditions and short residence times involved.

The advantage of non-intrusive (U)SAXS as compared with other techniques like photomicroscopy or electron microscopy is that the probe does not significantly alter the nucleation and growth conditions at the point of observation. In addition, the measured intensity is not influenced by the optical emission from the flame, unlike in light scattering.

In the current study (Sztucki *et al.*, 2007), soot particles formed in an acetylene diffusion flame at different flow rates between 90 ml min^{-1} and 130 ml min^{-1} have been investigated as a function of the height above burner (HAB) over a wide range of scattering vectors by combining complementary Bonse–Hart USAXS and pinhole SAXS measurements. Assuming ideal gas behavior, HAB can easily be converted into a residence time within the flame giving access to the growth dynamics of the soot particles.

The diffusion flame was produced by a homemade cylindrical stainless steel burner consisting of two concentric tubes (Sztucki *et al.*, 2007). The inner tube was fuelled by acetylene, the outer tube by a concentric laminar flow of nitrogen gas in order to stabilize the flame. In the flame, the development of multi-level structures can clearly be identified as a function of the height above the burner.

Fig. 8 shows a typical USAXS measurement recorded at HAB = 20 mm from an acetylene diffusion flame fuelled at 90 ml min^{-1} . In the figure the raw scattering data superimposed on the instrumental curve of the Bonse–Hart set-up are displayed. Comparing the low scattering intensity of this very dilute system (volume fraction $\varphi \simeq 10^{-6}$) with the high parasitic scattering of the monolithic Bonse–Hart channel-cut crystals (dashed line in Fig. 8) the investigation would not have been possible with the parasitic background level of a monolithic channel-cut set-up. The absolute scattering intensity $[I(q)]$ (inset of Fig. 8) is easily obtained by simple subtraction of the instrumental curve and following equation (2). The presented USAXS measurement is combined with pinhole SAXS data at higher q values as indicated. The inset also shows a fit to the measured data using the unified scattering function (Beaucage *et al.*, 2004; Sztucki *et al.*, 2007) which is a convenient approach to characterizing the scattering from systems with multiple structural levels (in this case up to three levels for primary particles, their aggregates, and larger agglomerates). The global scattering function combines the local scattering laws of each structural level in terms of a Guinier region followed by a power-law regime which is cut off by the characteristic size of the next smaller structures. The

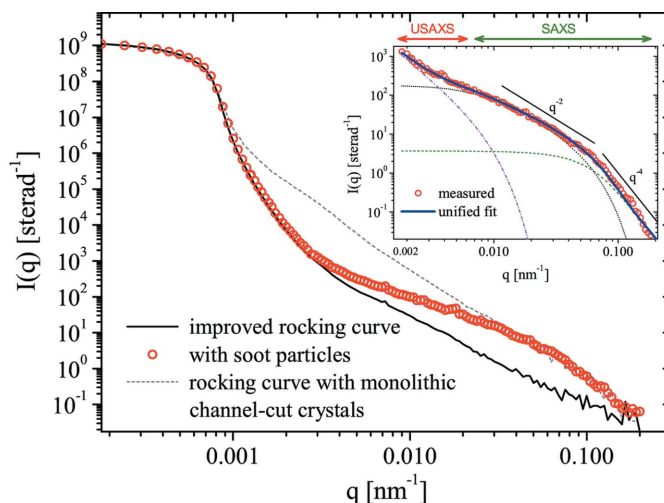


Figure 8

Typical USAXS from soot particles in a diffusion flame (acetylene, 90 ml min^{-1} , volume fraction $\varphi \simeq 10^{-6}$). The absolute scattering intensity $[I(q)]$ (inset) determined by USAXS is combined with pinhole SAXS data at larger q as indicated. The inset also shows a fit to the measured data by means of the unified scattering model for mass-fractal aggregates using three structural levels (see text for more details).

contribution of each of these structural levels to the unified fit is indicated by dashed or dotted lines in Fig. 8 (inset). At the largest q (pinhole SAXS range), primary particles of compact morphology (q^{-4} Porod slope) with a terminal size (radius of gyration) of about 27 nm are observed (Sztucki *et al.*, 2007). The morphology of mass-fractal aggregates of these primary particles could only be fully characterized using the data derived with the improved Bonse–Hart camera. These aggregates display a ramified structure with mass-fractal dimension ~ 2 ($\sim q^{-2}$ power law dependence) and a terminal radius of gyration of about 250 nm. At even smaller q values, scattering from agglomerates at least an order of magnitude larger than the aggregates and with a more compact morphology are detected going beyond the USAXS q range. A detailed analysis of the growth kinetics derived from the data recorded at different HAB and using different acetylene flow rates has been reported elsewhere (Sztucki *et al.*, 2007).

3.2. Casein micelles suspension

The usefulness of the reduced background of the USAXS instrument is demonstrated by another example involving a biological specimen which is susceptible to radiation damage. Fig. 9 shows the background-subtracted normalized intensities from a suspension of casein micelles from skimmed milk (BioLait, Lactel, France). Casein micelles constitute the main protein component of milk which has a highly self-assembled globular structure in the 100 nm range and substructures on the nanometer scale involving the different protein components and reticulated calcium phosphate nanoparticles (Holt *et al.*, 2003). The indicated concentration is the ratio of skimmed milk in the sample and not the exact volume fraction of casein micelles. In this case the sample is turbid in the visible region and also the casein micelles are highly poly-disperse. This makes USAXS a very useful technique but the

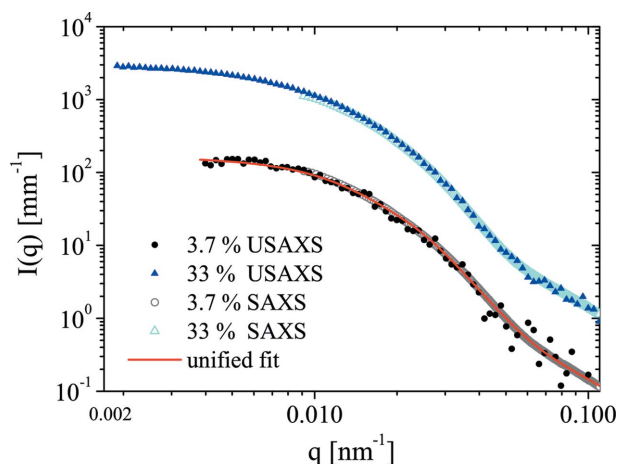


Figure 9

Normalized USAXS intensity from casein micelle suspensions (skimmed milk) at two different concentrations. For a comparison the corresponding data measured using a 10 m pinhole SAXS instrument are also shown. Bonse–Hart USAXS allows the structure and interactions between the large globular micelles, which form a turbid suspension in the visible region, to be determined. The continuous line is a fit to the unified scattering function with the following parameters: radius of gyration ~ 130 nm; polydispersity index ~ 7 ; corresponding to an average radius of about 60 nm.

sample is susceptible to radiation damage and in addition has low X-ray scattering contrast. The data in Fig. 9 were obtained by attenuating the beam intensity by a factor 15 (incident intensity $< 10^{11}$ photons s^{-1}). The low background nevertheless allowed sufficient intensity statistics to be obtained, even from a dilute suspension (3.7% of milk). The sample stability against radiation damage was verified by successive scans and their reproducibility.

The continuous line in Fig. 9 is a fit to the unified scattering function (Beaucage, Kammler & Pratsinis, 2004). The globular structure of micelles is described by a power law exponent of 4 (Porod behavior) (Pignon *et al.*, 2004). The resulting fit yields a radius of gyration of ~ 130 nm with polydispersity index ~ 7 , corresponding to an average radius of about 60 nm (Beaucage, Kammler & Pratsinis, 2004). The large polydispersity of micelles make the influence of the structure factor of intermicellar interactions less pronounced.

This example illustrates the applicability of USAXS for a dilute and low-contrast sample which is also radiation sensitive. The technique is useful for investigating structures of several hundred nanometers to the micrometer scale in turbid samples such as those involved in consumer products.

4. Conclusions and outlook

The quality of the surface finish of Si crystals in X-ray optics has a significant impact in many applications. One of them is Bonse–Hart USAXS where a parasitic scattering background in the wings of the rocking curves originates from the residual microstructures in the surface layer of the monolithic channel-cut crystals.

In this work, an optimized crystal design has been presented in order to reduce these problems. To overcome the limited

surface accessibility of channel-cut crystals during fabrication, the monolithic channel-cut crystals are replaced by double-crystal devices consisting each of two independent parallel crystals. A support with sub- μ rad resolution and high mechanical stability has been developed for the precise alignment of these so-called ‘double-crystal set-ups’.

The independent Si crystals were fabricated with the best possible surface finish at the ESRF crystal laboratory. The importance of mechano-chemical polishing of the conditioning crystals has been demonstrated: both the crystalline quality and the surface roughness are pivotal for reduction of the parasitic background and preservation of coherence. This could only be reached using deeply etched and highly polished crystals.

Concerning the analyzer stages which see only secondary scattering, the crystalline quality is more important than the microscopic surface roughness. Therefore, deep etching of the analyzer crystals is sufficient to reach optimum condition.

With the improvements presented above, the parasitic scattering background could be reduced by more than an order of magnitude to a comparable level of the background of an optimized pinhole SAXS instrument. This makes Bonse–Hart USAXS a very competitive complementary technique for SAXS investigations requiring very high angular resolution. The camera provides the possibility of recording SAXS over a wide dynamic range both in scattering vector \mathbf{q} and in intensity $I(q)$ (effectively up to eight orders of magnitude in intensity). With the latest improvements, the low q limit has been extended to 0.001 nm^{-1} (with $\lambda \simeq 0.1$ nm) and the instrument now allows the investigation of very low contrast and dilute systems. This has been demonstrated by the *in situ* study of soot particles in a diffusion flame.

It is possible that static and dynamic USAXS measurements can be recorded complementarily using a single experimental set-up. To exploit the improvements in instrumentation, a platform for online data processing and model fitting was developed.

The reported developments could also have considerable impact on emerging technologies for X-ray optics. For instance, the proposed design using deeply etched and highly polished crystals attempts to satisfy the conflicting requirements for imaging and scattering applications.

The double-crystal set-up could be used, for example, for the design of low-background monochromators. Fine tuning of the parallel alignment of crystals can be effective in compensating for heat load effects. The low-scattering background could be exploited in collimation devices for curtailing the parasitic background of long pinhole USAXS instruments (Yagi & Inoue, 2003) and refractive-lens-based focusing optics (Petukhov *et al.*, 2006).

Further improvement of the parasitic background scattering could be achieved by future advances in etching technology.

We thank P. Bösecke, P. Panine, E. Di Cola, D. Fernandez and A. Sole for support, and A. Freund, J. Ilavsky, O. Diat and J. Härtwig for discussions. The European Synchrotron

Radiation Facility is acknowledged for the provision of beam time and financial support.

References

- Agamalian, M., Christen, D. K., Drews, A. R., Glinka, C. J., Matsuoka, H. & Wignall, G. D. (1998). *J. Appl. Cryst.* **31**, 235–240.
- Beaucage, G., Kammler, H. K., Mueller, R., Strobel, R., Agashe, N., Pratsinis, S. E. & Narayanan, T. (2004). *Nature Mater.* **3**, 370–374.
- Beaucage, G., Kammler, H. K. & Pratsinis, S. E. (2004). *J. Appl. Cryst.* **37**, 523–535.
- Bonse, U. & Hart, M. (1965). *Appl. Phys. Lett.* **7**, 238–240.
- Bonse, U. & Hart, M. (1966). *Z. Phys.* **189**, 151–162.
- Diat, O., Bösecke, P., Ferrero, C., Freund, A. K., Lambard, J. & Heintzmann, R. (1995). *Nucl. Instrum. Methods Phys. Res. A*, **356**, 566–572.
- Harada, T., Matsuoka, H., Ikeda, T. & Yamaoka, H. (2000). *Colloids Surf. A*, **174**, 79–88.
- Holt, C., de Kruijff, C. G., Tuinier, R. & Timmins, P. A. (2003). *Colloids Surf. A*, **213**, 275–284.
- Ilavsky, J., Allen, A. J., Long, G. G. & Jemian, P. R. (2002). *Rev. Sci. Instrum.* **73**, 1660–1662.
- Konishi, T. & Ise, N. (1998). *Phys. Rev. B*, **57**, 2655–2658.
- Long, G. G., Jemian, P. R., Weertman, J. R., Black, D. R., Burdette, H. E. & Spal, R. (1991). *J. Appl. Cryst.* **24**, 30–37.
- Lyonnard, S., Belloni, L., Réus, V. & Zemb, T. (2000). *J. Appl. Cryst.* **33**, 582–586.
- Narayanan, T., Diat, O. & Bösecke, P. (2001). *Nucl. Instrum. Methods Phys. Res. A*, **467**, 1005–1009.
- Narayanan, T., Sztucki, M., Belina, G. & Pignon, F. (2006). *Phys. Rev. Lett.* **96**, 188301.
- Pedersen, J. S. (1995). *Modern Aspects of Small Angle Scattering*, edited by H. Brumberger, p. 57. Dordrecht: Kluwer.
- Petukhov, A. V., Thijssen, J. H. J., 't Hart, D. C., Imhof, A., van Blaaderen, A., Dolbnya, I. P., Snigirev, A., Moussaïd, A. & Snigireva, I. (2006). *J. Appl. Cryst.* **39**, 137–144.
- Pignon, F., Belina, G., Narayanan, T., Paubel, X., Magnin, A. & Gésan-Guiziou, G. (2004). *J. Chem. Phys.* **121**, 8138–8146.
- Pontoni, D. & Narayanan, T. (2003). *J. Appl. Cryst.* **36**, 787–790.
- Pontoni, D., Narayanan, T., Petit, J.-M., Grübel, G. & Beysens, D. (2003). *Phys. Rev. Lett.* **96**, 258301.
- Pontoni, D., Narayanan, T. & Rennie, A. R. (2002). *J. Appl. Cryst.* **35**, 207–211.
- Sánchez del Río, M. & Dejus, R. J. (1997). *Proc. SPIE*, **3152**, 148–157.
- Sztucki, M. (2007). *On-line processing and analysis of SAXS data*, <http://www.sztucki.de/SAXSutilities/>. (This program package is available in a compiled version without requiring a *Matlab* licence for Windows and Linux. Also available via <http://www.esrf.eu/UsersAndScience/Experiments/TBS/SciSoft/>.)
- Sztucki, M. & Narayanan, T. (2007). *J. Appl. Cryst.* **40**, s459–s462.
- Sztucki, M., Narayanan, T. & Beaucage, G. (2007). *J. Appl. Phys.* **101**, 114304.
- Sztucki, M., Narayanan, T., Belina, G., Moussaïd, A., Pignon, F. & Hoekstra, H. (2006). *Phys. Rev. E*, **74**, 051504.
- Yagi, N. & Inoue, K. (2003). *J. Appl. Cryst.* **36**, 783–786.